Title
Method—Practices and Pitfalls in Voltage Breakdown Analysis of Electrochemical Energy-Conversion Systems

Journal
Journal of The Electrochemical Society, 168(7)

ISSN
0013-4651

Authors
Gerhardt, Michael R
Pant, Lalit M
Bui, Justin C
et al.

Publication Date
2021-07-01

DOI
10.1149/1945-7111/abf061

Peer reviewed

Journal of The Electrochemical Society

The Electrochemical Society
Advancing solid state & electrochemical science & technology

OPEN ACCESS

Method—Practices and Pitfalls in Voltage Breakdown Analysis of Electrochemical Energy-Conversion Systems

To cite this article: Michael R. Gerhardt *et al* 2021 *J. Electrochem. Soc.* **168** 074503

Journal of The Electrochemical Society, 2021 **168** 074503

Method—Practices and Pitfalls in Voltage Breakdown Analysis of Electrochemical Energy-Conversion Systems

Michael R. Gerhardt,[1] Lalit M. Pant,[1,*] Justin C. Bui,[1,2] Andrew R. Crothers,[1,2,*] Victoria M. Ehlinger,[1,2,*] Julie C. Fornaciari,[1,2,*] Jiangjin Liu,[1] and Adam Z. Weber[1,,z]**

[1]*Energy Conversion Group, Energy Technologies Area, Lawrence Berkeley National Laboratory, Berkeley, California 94720, United States of America*
[2]*Department of Chemical and Biomolecular Engineering, University of California Berkeley, Berkeley, California, United States of America*

Many electrochemical energy-conversion systems are evaluated by polarization curves, which report the cell voltage across a range of current densities and are a global measure of operation and state of health. Mathematical models can be used to deconstruct the measured overall voltage and identify and quantify the voltage-loss sources, such as kinetic, ohmic, and mass-transport effects. These results elucidate the best pathways for improved performance. In this work, we discuss several voltage-breakdown methods and provide examples across different low-temperature, membrane-based electrochemical systems including electrolyzers, fuel cells, and related electrochemical energy-conversion devices. We present best practices to guide experimentalists and theorists in polarization-curve breakdown analysis.
 [DOI: 10.1149/1945-7111/abf061]

Manuscript submitted January 18, 2021; revised manuscript received March 10, 2021. Published July 23, 2021. *This paper is part of the JES Focus Issue on Proton Exchange Membrane Fuel Cell and Proton Exchange Membrane Water Electrolyzer Durability.*

Supplementary material for this article is available online

List of symbols

Roman

a	Specific surface area, cm^2/cm^3
a_j	Activity of species j
A	Area, cm^2
b	Tafel slope, 2.303 $RT/\alpha_c F$, V
c_j	Concentration of species j, M
D_{ij}	Binary diffusion coefficient between species i and j, cm^2/s
E^0	Standard reduction potential, V
E_r	Effectiveness factor
F	Faraday's constant, 96,485 C mol^{-1}
FE	Faradaic efficiency
i	Current density, A/cm^2
i_0	Exchange current density, A/cm^2
i_{lim}	Limiting current density, A/cm^2
I_{cell}	Cell current, A
k	Rate constant for chemical reaction
H_{O_2}	Henry's law constant for O_2 solvation, (Pa L)/mol
N_j	Molar flux of species j, mol/(cm^2 s)
p	Power density, W/cm^2
P	Pressure, Pa
P_j	Partial pressure of species j, Pa
q_k	Coefficient related to voltage loss mechanism k
R	Gas law constant, 8.314 J mol^{-1}
R_i	Rate of reaction or phase transition i, mol/(cm^3 s)
R'	Cell resistance, Ω
S_G,S_L	Gas-phase and liquid-phase saturation
T	Temperature, K
U	Equilibrium cell potential, V
U'	Effective cell potential, V
U^0_{cell}	Standard cell potential, V
V	Cell voltage, V
V_{OC}	Open circuit voltage, V
ΔV_k	Voltage loss due to mechanism k, V
v	Volume, cm^3
z_j	Charge of ion j

Greek

α_{eff}	Effective water transport coefficient for membrane and ionomer
α_a,α_c	Anodic and cathodic charge transfer coefficient
γ	Reaction order
η_C	Concentration overpotential, V
η_S	Surface overpotential, V
η_T	Total overpotential, V
κ	Ionic conductivity, S/cm
ξ	Electroosmotic coefficient
σ	Electronic conductivity, S/cm
ϕ	Potential

Superscripts and Subscripts

a	anodic
aCL	Anode catalyst layer
c	cathodic
cCL	Cathode catalyst layer
eff	effective
G	gas
I	Ionomer phase (including the membrane)
L	Liquid (including liquid electrolyte)
MEM	Membrane
ref	Reference
rxn	(Electro)chemical reaction
S	Solid phase (electronically conducting)

Electrochemical devices such as fuel cells and electrolyzers are promising renewable energy technologies with a wide range of applications. Optimizing the amount of power generated or

*Electrochemical Society Member.
**Electrochemical Society Fellow.
[z]E-mail: azweber@lbl.gov

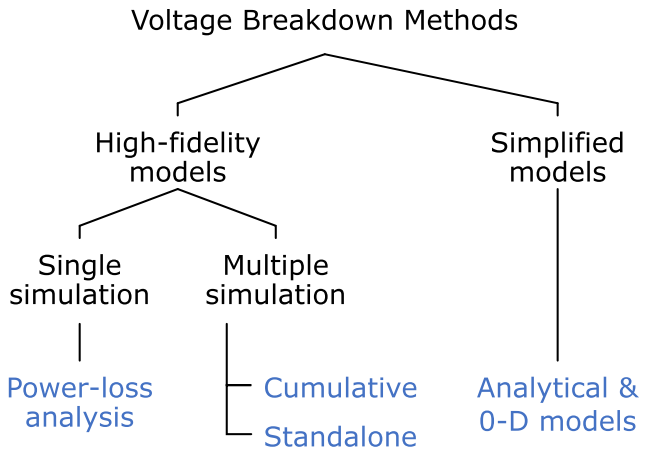

	$\sum \Delta V_k = V_{cell}$	Descriptive or Predictive	Sequence-Independent
Analytical & 0-D models	Yes	Descriptive	Yes
Cumulative	Yes	Predictive	No
Standalone	No	Predictive	Yes
Power-loss Analysis	Yes	Descriptive	Yes

Figure 1. A listing and comparison of the voltage breakdown methods used in this work.

consumed by these electrochemical devices can drive down costs and enable greater market penetration. Typically, polarization curves (current-voltage curves) are used to evaluate device performance under a wide range of experimental conditions. These polarization curves are easily accessible experimentally but difficult to interpret unambiguously.

Polarization curves can be qualitatively split into three regions: kinetic, ohmic, and mass-transport limited. In the kinetic region, which occurs at low current densities, the voltage loss increases exponentially with current density due to the form of the electrochemical kinetics. In the ohmic region the cell voltage changes linearly with current density in accordance with Ohm's law. In the mass-transport limited region the cell voltage again changes rapidly as the limiting current density is approached. The limiting current density is the current density at which one or more of the reactants on either electrode are depleted, which may occur due to fuel starvation or from cathode flooding in fuel cells. For galvanic cells, the cell voltage decreases as current increases, whereas for electrolytic cells, the cell voltage increases as current increases.

Voltage-breakdown techniques are often used in both experimental and modeling studies to identify and deconvolute the driving forces behind voltage losses evident in the polarization curve. A voltage breakdown is a method that takes as input a polarization curve $V(i)$ and returns a series of voltage losses $\Delta V_k(i)$, each of which can be assigned to one of the driving forces limiting electrochemical device performance. This procedure allows the kinetic, ohmic, and mass-transport regions of the polarization curve to be quantified. In addition, it provides insight into changes during operation when comparing different voltage curves.[1] Many sources of voltage loss are intrinsically coupled together, which complicates voltage-breakdown analysis. For example, increasing the conductivity of the ion-conducting phase in a porous electrode (that is, the ionomer in fuel cells) will cause a more uniform reaction distribution in the porous electrode, which may increase the kinetic voltage loss. Depending upon the method chosen these $\Delta V_k(i)$'s may or may not sum to the total voltage loss $V_{OC} - V(i)$ for all values of the current i.

In this work, we delineate the various methods for voltage breakdown analysis and discuss the interpretation of their results. We begin with a review of experimental and mathematical voltage-breakdown methods in the literature, followed by mathematical descriptions of some popular methods. We compare the application of several of these methods on a proton-exchange-membrane (PEM) fuel-cell model, then demonstrate the wide applicability of voltage-breakdown techniques to other low-temperature, membrane-based electrochemical systems by extending one method to electrolyzers and CO_2-reduction cells.

A Brief Review of Voltage Breakdown Methods

There is no standardized method for constructing voltage breakdowns. Newman and Thomas-Alyea[2] provide a primer on voltage breakdowns in general for electrochemical systems, sketching out how one might compute kinetic, ohmic, and concentration voltage losses for idealized systems such as concentric cylindrical electrodes. Specific to electrolyzers and fuel cells, mathematical modeling studies have been used to determine the individual contributions of cell components (that is, membrane, anode, cathode, gas diffusion layers, and so on) to voltage losses. For example, Bernardi and Verbrugge developed a mathematical model of a PEM fuel cell that calculates the cathode and anode overpotentials using Butler-Volmer equations.[3] Additionally, they were able to separate the membrane and electrode contributions to the ohmic losses of the cell. Marr and Li used a semi-empirical approach to calculate the ohmic resistance of the membrane, catalyst layers, and bipolar plates.[4] Baschuk and Li developed a model to incorporate the effects of flooding in the polarization curve.[5] Kulikovsky developed an analytical fuel-cell model to generate polarization curves in PEM fuel cells fit to experimental data under a variety of operating conditions.[6–8] An equivalent circuit model of a PEM fuel cell was created by Yu and Yuvarajan to predict voltage losses.[9] Baghalha et al. used a two-step deconvolution method in which each voltage loss is determined by removing the associated resistance and calculating the polarization curve.[10] Then, the new polarization curve is subtracted from the original polarization curve, which contains all of the resistances. A similar approach is used by Iczkowski and Cutlip[11] to analyze losses in the fuel-cell cathode. Secanell and coworkers [12,13] used the heat dissipation or the power loss from cell to estimate cell resistance and estimate corresponding voltage losses.

An experimental method to deconvolute experimental polarization curves into kinetic, ohmic, and mass-transfer losses was shown by Gasteiger[14] for PEM fuel cells and adapted to anion-exchange membrane fuel cells by Omasta.[15] This method first uses impedance spectroscopy to measure the resistance and extract the ohmic voltage loss, then uses low-current data to fit a Tafel slope, which is used to compute the kinetic voltage loss. The remaining voltage loss is assumed to relate to mass transport. Although this method is a useful diagnostic, it does not have a mathematical description of mass-transport voltage losses, thus leaving little guidance as to how to improve them (i.e., it is descriptive not predictive). Additionally, this method lumps the cathodic and anodic overpotentials into a single value. Detailed computational modeling can provide greater insight into the ultimate causes of these overpotentials and how to mitigate them.

Many experimental fuel-cell studies assume that the kinetic losses occur solely in the cathode, thereby assuming negligible

anode kinetic losses.[16–20] Later experimental studies sought to carry out a deeper analysis of voltage-loss contributions in the cell, as had been demonstrated in modeling studies. Williams et al.[19] published a method that deconvolutes the polarization curve into six cathode voltage-loss sources. The ohmic and mass-transport voltage losses are divided into electrode (that is, catalyst layer) and non-electrode components, such as the gas-diffusion layer (GDL) and membrane, accounting for four of the six sources. The kinetic voltage losses are divided into Tafel and activity components, accounting for the remaining two sources; anode electrode voltage loss is assumed negligible. The Tafel component of the kinetic voltage loss is assumed to scale logarithmically with current, whereas the activity component accounts for the difference between the equilibrium potential and the open circuit voltage (OCV) of a PEM fuel cell due to the unavoidable presence of parasitic reactions and gas crossover. Wood and Borup focused on separating the contributions of mass-transport overpotential from the cathode catalyst layer and GDL.[18] Flick et al.[17] reported the first measurement of anodic overpotentials by building upon the techniques introduced by Gasteiger et al.[16] and Wood and Borup,[18] and using a third electrically insulated reference electrode.

Voltage Breakdown Methods

Many methods exist for identifying sources of voltage loss in electrochemical systems through both models and experiments. In the next sections, we elaborate on several classes of voltage-breakdown methods and demonstrate their applications to several electrochemical systems. First, we discuss simplified analytical or zero-dimensional models of polarization curves that can be fit to available data. Then, we discuss methods applicable to high-fidelity multiphysics models, from which simple expressions for each voltage loss are more difficult to derive. In these cases, one can choose between multiple-simulation methods, in which voltage loss mechanisms are identified by changing the input parameters that define them, and single-simulation methods, in which the model solutions are post-processed into a series of voltage losses. These methods and their key features are summarized in Fig. 1.

Analytical and 0-D models.—Analytical models of polarization curves usually report the cell voltage V as a function of current density i and some fitting parameters. By fitting an analytical model like those discussed below to experimental data, simple voltage breakdowns can be rapidly obtained. The simplest voltage breakdown can be written as[21]

$$V(i) = U - \Delta V_{\text{kinetic}}(i) - \Delta V_{\text{ohmic}}(i), \quad [1]$$

where V is the cell voltage, U is the equilibrium cell potential, and $\Delta V_{\text{kinetic}}$ and ΔV_{ohmic} are the kinetic and ohmic voltage losses, respectively. The kinetic voltage loss can be described mathematically using a Tafel kinetics expression,

$$\Delta V_{\text{kinetic}} = b \log \frac{i}{i_0}, \quad [2]$$

where i_0 is the exchange current density, i is the superficial current density, and b is the Tafel slope, which is defined as

$$b = 2.303\frac{RT}{\alpha_c F}, \quad [3]$$

where R is the ideal gas constant, T is the temperature, F is Faraday's constant, and α_c is the cathodic transfer coefficient. The ohmic voltage loss can be described using Ohm's law,

$$\Delta V_{\text{ohmic}} = R'i, \quad [4]$$

where R' is the overall cell resistance. Replacing $\Delta V_{\text{kinetic}}$ and ΔV_{ohmic} in Eq. 1 with their definitions in Eqs. 2 and 4 results in the following equation for the cell voltage as a function of current density:

$$V = U' - b \log i - R'i, \quad [5]$$

where $U' = U + b \log i_0$. The parameters b, i_0, and R' can be determined by fitting the measured polarization curve.

Defining a mass-transport voltage loss is more challenging. Chamberlin et al.[22] and Kim et al.[23] extended Eq. 5 to account for mass-transport voltage losses by including the deviation from the linear behavior predicted by ohmic losses:

$$V(i) = U' - b \log i - R'i - g \exp(hi), \quad [6]$$

where g and h are fitting parameters. The overall voltage breakdown equation becomes

$$V(i) = U' + \Delta V_{\text{kinetic}}(i) + \Delta V_{\text{ohmic}}(i) + \Delta V_{\text{mass transport}}(i). \quad [7]$$

The mass-transport voltage loss is defined as

$$\Delta V_{\text{mass transport}}(i) = -g \exp(hi). \quad [8]$$

Lee et al. introduced an additional term to this equation to account for the effect of gas pressure and oxygen concentration on the fuel-cell performance,

$$\text{V(i)} = U' - b \log i - R'i - g \exp(hi) - b \log\left(\frac{P}{P_{O_2}}\right), \quad [9]$$

where P is the gas pressure and P_{O_2} is the partial pressure of oxygen;[24] the above assumed a first order dependence on oxygen. Alternatively, mass-transport losses can be written in terms of the limiting current density, i_{lim},[25–27]

$$V(i) = U' - b \log i - R'i + b \log\left(1 - \frac{i}{i_{\text{lim}}}\right), \quad [10]$$

with the mass-transport voltage loss defined as

$$\Delta V_{\text{mass transport}}(i) = b \log\left(1 - \frac{i}{i_{\text{lim}}}\right). \quad [11]$$

While this approach has a more physical basis and requires fewer fitting parameters than Eq. 8, this model often results in a poorer fit of experimental data due to the reduced number of fitting parameters and implicitly assumes an easily measurable mass-transfer limiting current density, which is not always the case since in fuel cells there is a finite voltage window and in electrolyzers other effects such as resistive heating occur at high current densities.

In general, 0-D models are reliant upon fit to experimental data, and few parameters can be extracted from these models. 0-D models give poor predictions of cell performance outside of the fit conditions because they exclude geometric effects and ignore the interdependence of the various sources of resistance, such as the coupling between ionic conductivity and electrochemical kinetics discussed above. These methods are useful for an initial or empirical characterization of a system, but they cannot provide much insight into the underlying driving forces leading to voltage losses or identify the location in the fuel cell at which these losses occur. Their predictive power remains limited to similar conditions upon which they were fit.

Sequential limiting-case analysis.—A physics-based computational model of an electrochemical system can be used to generate polarization curves and obtain voltage breakdowns. In these higher-dimensional models, however, the voltage output is typically a complicated, implicitly defined function of many input parameters, rather than an explicitly defined function of current as in the 0-D models described above. Thus, some ambiguity exists in deriving the voltage breakdown, and several approaches are used.

One common method of identifying the voltage loss associated with a specific loss mechanism is to compute the polarization curve twice: a "baseline" analysis including the performance-limiting mechanism and a "limiting-case" analysis with the mechanism removed, usually by setting the relevant transport or kinetic coefficient to an arbitrarily high value. For example, to illustrate the effect of oxygen diffusion, a simulation with arbitrarily large oxygen diffusivity could be compared to a simulation under standard conditions. The difference in cell behavior between the two analyses is then attributed to the mechanism in question. Thus, the voltage loss associated with a mechanism k can be given as

$$\Delta V_k(i) = V(i)|_{(\ldots, q_k=\infty, \ldots)} - V(i)|_{(\ldots, q_k\neq\infty, \ldots)}, \qquad [12]$$

where i is the current density and q_k is the coefficient associated with the *kth* loss mechanism, typically a diffusivity, conductivity, or exchange current density. The voltage breakdown is then a listing of ΔV_k values for all k mechanisms. There are two popular methods for performing a voltage breakdown using this limiting-case technique, which we term the "cumulative" method and the "standalone" method.

In the following subsections, we show examples of performing cumulative and standalone voltage breakdowns in PEM fuel cells using an in-house developed 2-D physics-based model.[28] The details of the physics, mathematical framework and simulation parameters of the model are given in the original article. Although most of the model is used as described in the article, a few changes have been made for this work: first, the cathode catalyst specific area (a_c) has been assumed to be humidity independent and fixed at 5×10^4 cm^2/cm^3; and second, the cathode oxygen-reduction-reaction (ORR) kinetics has been changed from Tafel kinetics to Butler-Volmer kinetics since the Tafel kinetics equation is only valid when the overpotential is large. During limiting-case analysis, however, the ORR kinetics is increased, resulting in relatively small overpotentials and non-physical results using Tafel kinetics at low current density.

Cumulative limiting-case analysis.—The cumulative voltage-loss analysis is based on performing cumulative limiting-case analyses with each loss mechanism to obtain the total voltage loss. In this method, a baseline polarization curve is obtained first, and one voltage-loss mechanism is removed as described above (Eq. 12). Then, another voltage-loss mechanism is eliminated, and the simulation repeated, until all voltage-loss mechanisms are removed. For example, for the removal of the first voltage-loss mechanism, hydrogen diffusivity can be set to an arbitrarily high value to remove hydrogen transport limitations, and the polarization curve can be recalculated. The difference between the new polarization curve and the original curve will show the voltage loss associated with hydrogen transport. For the next simulation, hydrogen and oxygen diffusivities can *both* be set to arbitrarily high values, and the difference between this third polarization curve and the prior one can be assigned to oxygen transport. The value of the oxygen-transport voltage loss is conditional upon the removal of the hydrogen-transport voltage loss. An example result of this method can be seen in Fig. 2, in which each colored slice shows the voltage loss associated with a particular-loss mechanism. In general, the total voltage loss associated with a total of n mechanisms in a cumulative limiting analysis can be given as

$$\begin{aligned}\Delta V(i) = \sum_{k=1}^{n} \Delta V_k(i) = &\underbrace{\left(V(i)|_{(q_1=\infty,\, q_2,q_3,\ldots q_k,\ldots,\, q_n)} - V(i)|_{(q_1,\, q_2,q_3,\ldots,\, q_k,\ldots,q_n)}\right)}_{\text{1st mechanism loss}} \\ &+ \underbrace{\left(V(i)|_{(q_1=\infty,\, q_2=\infty,q_3,\ldots,q_k,\ \ldots,q_n)} - V(i)|_{(q_1=\infty,\, q_2,q_3,\ \ldots,q_k,\ \ldots,q_n)}\right)}_{\text{2nd mechanism loss}} \\ &+ \cdots \\ &+ \underbrace{\left(V(i)|_{(q_1=\infty,\, q_2=\infty,q_3=\infty,\ldots,q_k=\infty,\ \ldots,q_n=\infty)} - V(i)|_{(q_1=\infty,\, q_2=\infty,\, q_3=\infty,\ldots,q_k=\infty,\ldots,q_n)}\right)}_{\text{nth mechanism loss}} \\ &= \underbrace{\left(V(i)|_{(q_1=\infty,\, q_2=\infty,q_3=\infty,\ldots,q_k=\infty,\ \ldots,q_n=\infty)}\right)}_{V_{OC}} - \underbrace{V(i)|_{(q_1,\, q_2,q_3,\ldots q_k,\ldots,\, q_n)}}_{\text{cell potential}}. \end{aligned} \qquad [13]$$

It can be observed that all the different loss mechanisms ΔV_k's sum to the total voltage loss ΔV. Note that ΔV_k is dependent not only on mechanism k, but on the choice of mechanisms removed or left in place (i.e. order matters).

Using this method, cumulative limiting-case analysis of voltage loss was performed as shown in Fig. 2. First, the polarization curve was obtained with a base-case parameter set (that is, none of the loss mechanisms were eliminated). Then each voltage-loss mechanism was removed by increasing its associated coefficient to an arbitrarily large value. The coefficient increment factors for each loss mechanism and the sequence by which the mechanisms were eliminated are shown in Table I. Ideally, the increment factors should be infinitely large to eliminate the losses associated with that mechanism, but that is not possible in a numerical model. In this work, the coefficients were increased until the model outputs showed an asymptotic behavior and changed negligibly, or if an upper limit was reached for which the model showed numerical instability. As shown in Table I, all the parameters except anode exchange current density were increased by a factor of 10^{10}, where any further increase showed negligible impact of model output. The anode exchange current density was only increased by a factor of 10^5, as any further increase resulted in numerical instability in the model. For the cumulative analysis, removing all the limiting mechanisms is also not possible, as it leads to singularities and numerical instability. Therefore, for a n-mechanism based analysis, only $n-1$ limiting mechanisms are cumulatively eliminated and the rest of the losses can be attributed to the n^{th} mechanism as shown in Eq. 13. Since different voltage-loss mechanisms dominate under different operating conditions, the voltage-loss analysis was performed under four sets of operating conditions where each loss mechanism can be properly highlighted: dry, humid, oxygen-limited, and flooded.

As seen in Fig. 2, the cumulative limiting-case analysis is sensitive to operating conditions and can help identify causes of poor cell performance. For example, comparing Figs. 2a and 2b reveals that the higher RH case exhibits much lower ohmic voltage losses within the membrane

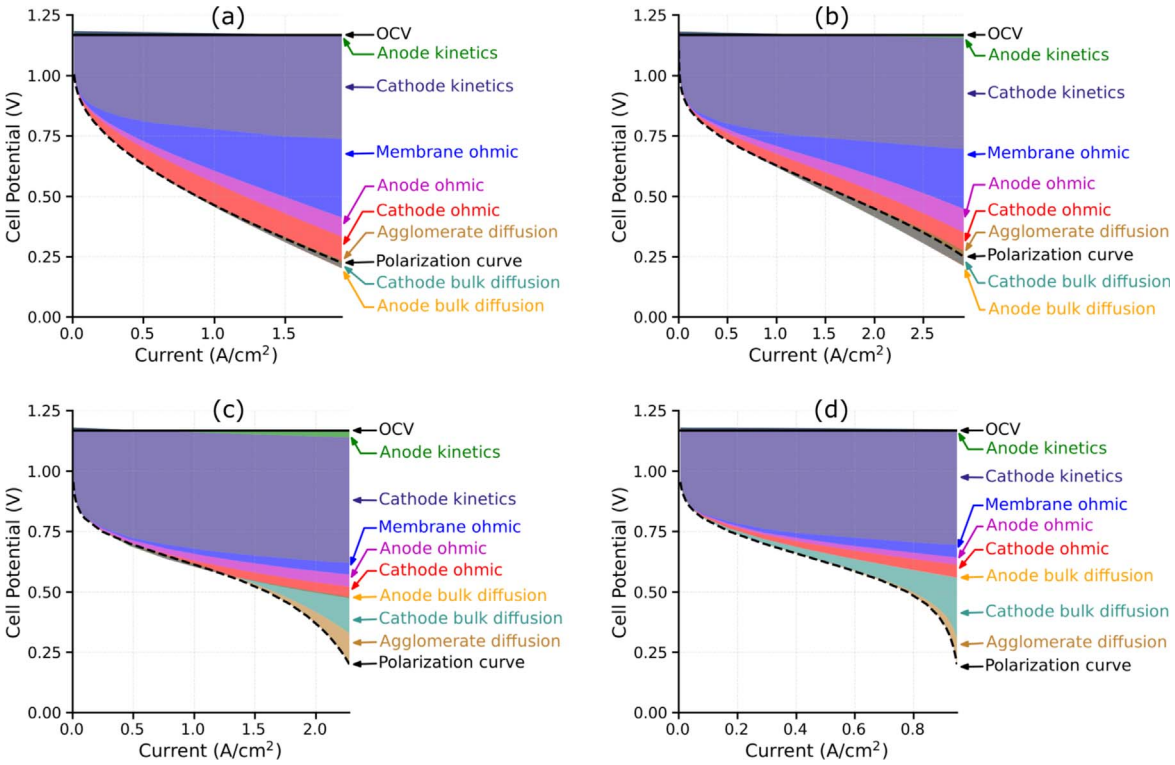

Figure 2. Cumulative limiting-case voltage breakdown analysis of a PEM fuel cell model at different operating conditions. Voltage loss regions and labels are color-coordinated. (a) Dry: 80 °C, 40% RH and air (21% O_2) in cathode; (b) Humid: 80 °C, 80% RH and air in cathode; (c) Flooded: 80 °C, 100% RH and air in cathode; (d) Oxygen-limited: 80 °C, 100% RH and 5% O_2 in cathode.

and cathode ionomer, resulting in a near-doubling of the current density at 0.5 V and an increase of 1 A cm^{-2} at 0.25 V when the RH is increased from 40% to 80%. Interestingly, increasing anode and cathode bulk diffusion coefficients in the 40% and 80% RH cases results in a predicted voltage *loss* rather than a gain, causing the voltage breakdown to extend below the initial polarization curve. This phenomenon can be attributed to the increase in water transport away from the membrane and catalyst layers due to faster water diffusion, which results in a slight drying out of the membrane and ionomer relative to the base case. This drying out, in turn, causes a voltage loss because the properties of the ionomer are extremely hydration-dependent.[28,29]

By simulating flooding conditions, as in Figs. 2c and 2d, mass-transport losses can be accentuated. In these cases, ohmic losses are significantly reduced because the membrane is well-hydrated, but diffusion losses are increased due to the reduced pore space caused by flooding at the cathode. The effects of slower oxygen transport manifest as nonlinear cathode diffusion voltage losses at high current density, and these losses are exacerbated at low oxygen concentration as shown in Fig. 2d. The cumulative limiting-case analysis breakdown allows researchers to quantify those mass-transport losses and assign them to bulk cathode diffusion, which is influenced by the structure of the catalyst layer, and agglomerate diffusion, which is influenced by the properties of the ionomer and the size of the agglomerates. Researchers can then choose which of these effects is more important to mitigate and prioritize research and development activities toward that effect. Thus, voltage breakdowns can help guide fuel-cell research and development at both beginning and end of life.

Table I. List of control parameters and their increase factors for different loss mechanisms. The order of elimination for the parameters in different cumulative analysis is also shown. The voltage losses for last parameter (8) are estimated by eliminating the other 7 losses from total voltage loss.

Parameter	Sequence/order of removal in cumulative analysis		Increase factor for parameter (infinity limit) $q_{(k,\infty)}/q_{(k,0)}$
	1st analysis	2nd analysis	
Oxygen diffusivity in agglomerate ($D_{O_{2,M}}$)	1	6	10^{10}
Effective diffusivity in cathode porous media ($D_{ij,c}^{eff}$)	2	5	10^{10}
Effective diffusivity in anode porous media ($D_{ij,a}^{eff}$)	3	4	10^{10}
Effective cathode CL ionomer conductivity (κ_{cCL}^{eff})	4	2	10^{10}
Effective anode CL ionomer conductivity (κ_{aCL}^{eff})	5	3	10^{10}
Effective membrane ionomer conductivity (κ_{mem}^{eff})	6	1	10^{10}
Cathode ORR exchange current density ($i_{0,c}$)	7	8 (remainder)	10^{10}
Anode HOR exchange current density ($i_{0,a}$)	8 (remainder)	7	10^{5}

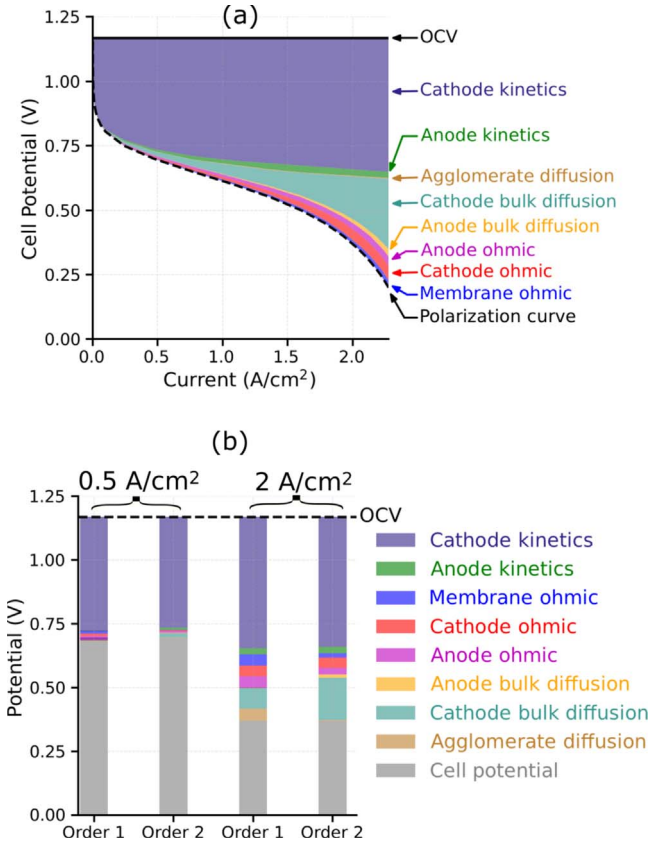

Figure 3. (a) Cumulative limiting-case analysis for a PEM fuel cell under identical conditions as Fig. 2c (80 °C, 100% RH, air), but with a different sequence of limit removals. (b) Comparison of voltage breakdowns at two different current densities for the two different sequences of limit removals. Importantly, the sequence matters; removing the anode kinetic limit first results in greatly increased estimation of anode kinetic voltage losses, for example.

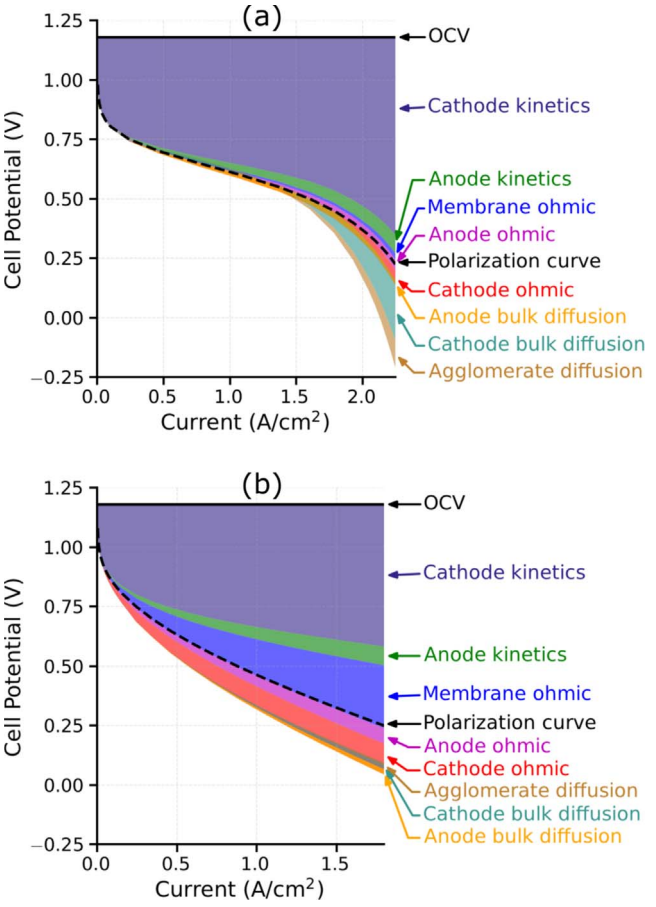

Figure 4. Voltage breakdown calculated from standalone limiting-case analysis for a PEM fuel cell under identical conditions as (a). Figs. 1c and 2a (80 °C, 100% RH, air) and (b). Figure 2a (80 °C, 40% RH, air). Note that the predicted voltage losses do not sum to the total voltage loss.

Care must be taken in performing and interpreting a cumulative limiting-case analysis voltage breakdown. As discussed earlier, in a cumulative limiting-case analysis, the voltage loss ΔV_k due to mechanism k depends on the choice of other mechanisms removed or left in place. Therefore, the sequence in which voltage losses are removed impacts the resultant voltage breakdown. For example, cathode bulk diffusion losses appear much larger in Fig. 3, in which those losses are removed before agglomerate diffusion losses, than in Fig. 2c, in which agglomerate diffusion losses are removed first. While both analysis were performed at same conditions, the difference in the results arises from the different parametric conditions under which cathode bulk diffusion losses are removed in each figure: in Fig. 2c, the "cathode bulk diffusion voltage loss" represents the voltage loss due to finite cathode bulk diffusion in the presence of infinitely fast agglomerate diffusion, whereas in Fig. 3, agglomerate diffusion is not infinitely fast when cathode bulk diffusion losses are removed. These voltage losses are not necessarily identical because the phenomena in question are significantly coupled within the porous electrode. For example, improving cathode bulk diffusion first artificially increases the concentration of oxygen available to the cathode catalyst agglomerates, thereby enhancing agglomerate mass transport without changing the oxygen diffusivity within the agglomerate. The impact of limit removal sequence on voltage loss due to other phenomena can also be observed in Fig. 3b. In some sense, the dependence on which one is removed first shows the coupling of the different resistances on the aggregated behavior.

Standalone limiting-case analysis.—One way to avoid ambiguities associated with the order in which voltage losses are explored is to consider only one voltage loss mechanism at a time. This voltage breakdown method, which we call standalone limiting-case analysis, focuses on the individual impact of each mechanism on the cell potential. This analysis is similar to that of Baghalha et al.[10] and Iczkowski and Cutlip.[11] With this method, the voltage loss due to a mechanism k is always obtained in comparison to the normal polarization curve:

$$\Delta V_k(i) = V(i)|_{(q_1,q_2,q_3,\ldots,q_k=\infty,\ldots,q_n)} - V(i)|_{(q_1,q_2,q_3,\ldots,q_k,\ldots,q_n)}. \quad [14]$$

The standalone method ignores coupling between different loss mechanisms, such as a change in electrochemical kinetics causing a shift in the reaction zone affecting mass transport. Therefore, the sum of voltage losses $\sum \Delta V_k$ computed by the standalone method may not equal the total voltage loss $V_{OC} - V(i)$. Essentially, the standalone method demonstrates the maximum voltage change upon removing each single limit, whereas the cumulative method demonstrates the expected change in performance upon removing a sequence of limits. Thus, the former is perhaps better at explaining single phenomena whereas the latter considers the interactions and is perhaps better for understanding the sensitivity of the system.

Examples of voltage breakdowns produced using the standalone method are shown in Fig. 4. In this case, the sum of predicted

voltage losses is larger than the total simulated voltage loss, indicating that the different mechanisms are interrelated and therefore cannot be linearly superimposed. Thus, increasing a single coefficient does not necessarily impact only a single limiting mechanism. For example, when ionomer proton conductivity is increased, ionomer ohmic losses decrease, which in turn reduces the kinetic overpotentials, thereby decreasing the kinetic losses. Similarly, increasing diffusion coefficients decreases the bulk diffusion losses as well as kinetic losses. Adding all the individual voltage losses therefore overestimates the total voltage loss as some of the losses are overcounted.

Additionally, the standalone analysis gives quantitatively different voltage loss values than the cumulative analysis. For example, Fig. 4a shows the standalone voltage breakdown under identical conditions to Figs. 2c and 3a. The cathode kinetics losses, anode kinetics losses and agglomerate losses in the standalone analysis are much higher, due to the interrelation mentioned previously. Similarly, Fig. 4b shows a standalone voltage breakdown under identical conditions to Fig. 2a. For this case as well, cathode and anode kinetics losses are higher in the standalone analysis than in the cumulative analysis. In both cases, ohmic losses are generally lower for standalone analysis compared to the cumulative cases. From these comparisons it can be inferred that increasing the protonic conductivity of the CLs and membrane has less impact by itself than in conjunction with gas diffusion properties (Fig. 2). When the gas diffusion coefficients are increased, the reactions move closer to the membrane/CL interface, thereby reducing the ohmic losses in the CLs. Then, increasing the membrane and ionomer conductivities eliminates any remaining ohmic losses. In summary, the standalone analysis demonstrates which single parameter limits the cell performance most, whereas the cumulative analysis can find which combinations of parameters limit performance improvement.

Power-loss post-processing method.—In principle, voltage breakdowns can be obtained from the output of a single simulation without running any additional simulations, because all sources of voltage loss are implicitly defined within the model framework. In practice, the deconvolution of the overall voltage loss into its various sources using postprocessing methods is challenging, because each source of loss must be clearly defined and appropriately averaged over space. This approach was first applied in terms of resistance breakdown and heating by Secanell and coworkers.[12,13]

One framework for enumerating the voltage losses in an electrochemical system is to consider *power* losses (i.e., rates of energy loss). These power losses can then be normalized by the cell current to define a voltage loss. The power-density vector at any point in the cell is defined as the product of current density and the potential difference from that point to a reference potential ϕ_k^{ref},

$$\boldsymbol{p_k} = \mathbf{i}(\phi_k - \phi_k^{\text{ref}}), \qquad [15]$$

where ϕ_k^{ref} is often set to the anode or cathode current collector potential. The divergence of power density, $\nabla\cdot\boldsymbol{p_k}$, is the "loss" of power, with units of volumetric power, and represents generation of waste heat. The power losses for each hypothesized mechanism k is the integral of $\nabla\cdot\boldsymbol{p_k}$ over the relevant spatial volume v_k. From this integral, the voltage loss due to mechanism k can be derived if the cell current I_{cell} is known,

$$\Delta V_k = \frac{\int_{v_k} \nabla\cdot\boldsymbol{p_k}\, dv_k}{I_{cell}}. \qquad [16]$$

From the divergence theorem, the net power loss across the volume is equal to the power density leaving v_k integrated over the surface of v_k, S_k,

$$\int_{v_k} \mathbf{i}\cdot\nabla\phi_k dv_k + \int_{v_k} (\phi_k - \phi_k^{\text{ref}})\nabla\cdot\mathbf{i} dv_k = \int_{S_k} \boldsymbol{p}\cdot\boldsymbol{n} dS_k = I_{\text{cell}}\Delta V_k, \qquad [17]$$

where $\boldsymbol{n}$ is the vector unit normal to S_k. If v_k is a layer of the cell sandwich, all of the cell current passes through S_k and we arrive at the second equality. From Eq. 15, the voltage loss due to mechanism k is defined as $\Delta V_k \equiv \int_{S_k} \boldsymbol{i}\cdot\boldsymbol{n}\phi dS_k / I_{cell}$. For the case of a rectangular volume with two parallel sides at constant potentials, ΔV_k reduces to the potential difference between the two sides. This method robustly defines voltage drops across interfaces with non-uniform potentials and is valid for complex or rough surfaces. Furthermore, this method can easily be simplified from the 3-D derivation given here to lower-dimensional models, and has been used with 1-D and 2-D models as well as a 2-D model with a channel-stepping algorithm to study down-channel effects.[30–32]

Contrary to the limiting-case methods described above, which require multiple runs of a simulation, this power-loss analysis-based method demands derivation of mathematical expressions for the voltage loss contributions but only requires a single simulation. Typically, these expressions come from constitutive equations that relate $\mathbf{i}$ to $\nabla\phi_k$ and $\nabla\cdot\mathbf{i}$ to $\phi_k - \phi_k^{ref}$, such as Ohm's law or the Butler-Volmer equation, respectively. Following Eq. 17, the individual voltage-loss contributions are defined as follows. In these definitions, we use terminology typically associated with fuel cells and electrolyzers, such as "catalyst layer (CL)" and "membrane" to describe the relevant volumes v_k. In other electrochemical systems, these are sometimes called "electrode" to denote a reacting surface, and "electrolyte" to denote an ion conductor. The Supplemental Information lists details and explicit derivations of the power-loss terms used in each model in this work.

The first term on the left side of Eq. 17 accounts for power losses due to ohmic resistances that introduce a voltage gradient. If $\nabla\phi_k$ is replaced with $\frac{i}{\kappa}$, as would be expected for an ohmic resistor, the integrand represents the power dissipated by such a resistor. Thus, the voltage loss due to ohmic resistances within the membrane and ionomer can be estimated as

$$\Delta V_{ohmic} = \frac{\int_{\text{CL+MEM}} \frac{\boldsymbol{i_I}\cdot\boldsymbol{i_I}}{\kappa^{\text{eff}}} dv_{\text{CL+MEM}}}{I_{cell}}, \qquad [18]$$

where $\boldsymbol{i_I}$ is the local ionic current density in A cm^{-2} and κ^{eff} is the effective ionic conductivity of the ionomer. In the models studied here, a coupled ion- and water-transport approach is used, meaning that electroosmosis also influences the potential gradient.[33] Thus, in the calculations of ΔV_{ohmic} in this work, we use

$$\Delta V_{ohmic} = \frac{\int_{\text{CL+MEM}} \left[\frac{\boldsymbol{i_I}\cdot\boldsymbol{i_I}}{\kappa^{\text{eff}}} - \frac{\xi}{F\alpha_{\text{eff}}}\left(\boldsymbol{i_I}\cdot\boldsymbol{N}_{\mathbf{H_2O,I}} - \frac{\xi}{F}(\boldsymbol{i_I}\cdot\boldsymbol{i_I})\right)\right] dv_{\text{CL+MEM}}}{I_{cell}}. \qquad [19]$$

In Eq. 19, α_{eff} represents the effective water transport coefficient,[33] $N_{H_2O,I}$ is the molar flux of water within the membrane and ionomer, and ξ is the electroosmotic coefficient.

The second term on the left side of Eq. 17 accounts for kinetic and mass-transport losses associated with an electrochemical reaction. By considering both electronic and ionic currents and referencing the potentials to the standard reduction potential of the

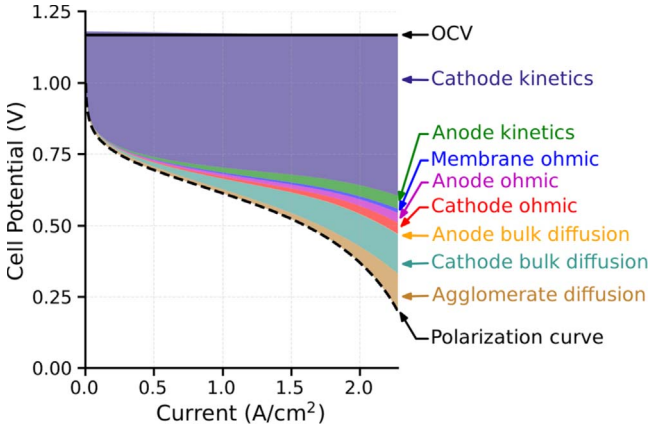

Figure 5. PEM fuel cell voltage breakdown by the power-loss analysis method. The polarization curve was computed under identical conditions as Fig. 2c (80 °C, 100% RH, air cathode).

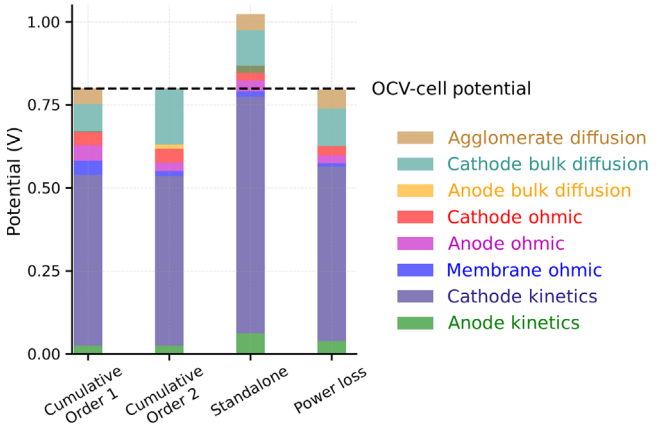

Figure 6. Comparison of different voltage loss breakdown methods in the PEM fuel cell model at 2 A cm^{-2}.

electrochemical reaction, the integrand can be shown to equal $\eta_T i_{rxn}$, where $\eta_T = \phi_S - \phi_I - E^0$ is the overpotential. Thus, a "total" voltage loss can be defined that encompasses all kinetic and mass-transfer effects at the given electrode:

$$\Delta V_{total} = \frac{\int_{CL} i_{rxn}\eta_T dv_{CL}}{I_{cell}} \quad [20]$$

To gain further insight into the voltage-loss mechanisms, the overpotential η_T can be split into a kinetic portion and a mass-transport portion.

$$\eta_T = \eta_S + \eta_C \quad [21]$$

These portions are often called the surface overpotential η_S and the concentration overpotential, η_C.

The kinetic voltage losses are defined by integrating the power loss due to the surface overpotential η_S over the volume of each catalyst layer and dividing by the total current density:

$$\Delta V_{\text{kinetic}} = \frac{\int_{CL} i_{\text{rxn}}\eta_S dv_{\text{CL}}}{I_{cell}} \quad [22]$$

where i_{rxn} is the local volumetric current source. The surface overpotential η_S is determined by the expression for electrochemical kinetics used in the model and is the difference between the local potential of the electrode and the equilibrium potential of an identical electrode given the same local reactant and product concentration without any flowing current.

The mass-transport voltage loss is the voltage loss associated with the change in reactant concentration from a reference concentration $c_{j,ref}$ to its value at the electrode surface c_j. The reference concentration $c_{j,ref}$ is usually the value of c_j at the cell inlet boundary. The mass-transport voltage loss can be calculated by subtracting the kinetic voltage loss in Eq. 22 from the total voltage loss. Usually, the mass-transport voltage loss takes the form:

$$\Delta V_{\text{mass transport,j}} = \frac{\int_{CL} i_{rxn}\frac{RT}{\alpha F}\ln\left(\left(\frac{c_j}{c_{j,ref}}\right)^{\gamma}\right)}{I_{cell}}, \quad [23]$$

for each chemical species j, where c_j and $c_{j,ref}$ represent the local and reference concentration, respectively, and γ represents the reaction order. For ideal gaseous reactants, the partial pressure P_j of each species can be used in place of the concentrations c_j.

A common feature in many fuel-cell models, including the one used as a demonstration in this work, is the use of an agglomerate model,[34] which considers the cathode catalyst layer comprised of spherical agglomerates of catalyst particles sheathed in a layer of ionomer that inhibits oxygen transport. This agglomerate model assumption adds a mass-transport related voltage loss arising from diffusion within the agglomerate and through the ionomer film surrounding the agglomerate. This voltage loss can be expressed as

$$\Delta V_{agglomerate} = \frac{\int_{CL} -i_{rxn}\frac{RT}{\alpha_C F}\ln\left(\left(\frac{c_{O_2,ref}H_{O_2}}{P_{O_2,ref}}\right)\left(\frac{c_{O_2\,film|gas}}{c_{O_2,core|film}}\right)\left(\frac{1}{E_r}\right)\right)}{I_{cell}}, \quad [24]$$

where E_r is the effectiveness factor, $c_{O_2,ref}$ and $P_{O_2,ref}$ are the reference concentration and pressure of oxygen, H_{O_2} is the Henry's law constant for dissolution of oxygen into the ionomer film, and the remaining terms are the oxygen concentration at the gas/film interface and the film/core interface. If one desires an even more fine-grained approach, each fraction within the natural logarithm can be broken out into its own voltage loss.

An example of a power-loss analysis voltage breakdown is shown in Fig. 5a. Like the standalone method, the power-loss analysis method does not depend on the sequence of limit removals. Furthermore, it does not require multiple simulations, which can reduce computational time and cost. However, this method focuses on the instantaneous operation of a cell rather than defining the expected improvement in cell performance upon removing a specific limit, which could obscure some of the synergistic or coupled interactions between phenomena and variables. Thus, this method has quantitatively different predictions than either of the limiting-case analyses. This method also requires derivation of explicit mathematical definitions of the voltage losses, which can be challenging, if not impossible, depending upon the equations used in the model.

Finally, as noted in Fig. 1 and above discussions, there are several different ways to accomplish the voltage-loss breakdowns, with the cumulative being more predictive or similar to sensitivity analysis and the power loss being more descriptive. A more detailed comparison is shown in Fig. 6, which also highlights the dependence of the cumulative method on the order of limit removal.

Voltage Breakdowns in Other Electrochemical Systems

The voltage breakdown methods are not limited to fuel cells and can be applied to a wide variety of electrochemical energy-conversion technologies. This section illustrates some examples of voltage breakdowns in PEM electrolysis, anion-exchange-membrane (AEM) electrolysis, and electrochemical CO_2 reduction using the power-loss methodology. Each approach adds certain nuances to

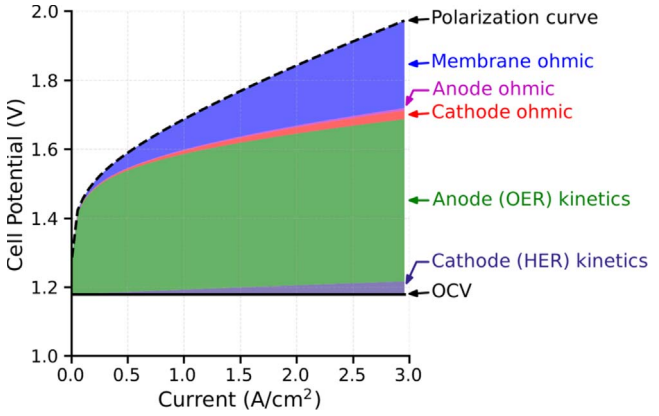

Figure 7. PEM electrolzyer applied-voltage breakdown, indicating the largest loss is within the anode kinetics (green) and PEM (blue).

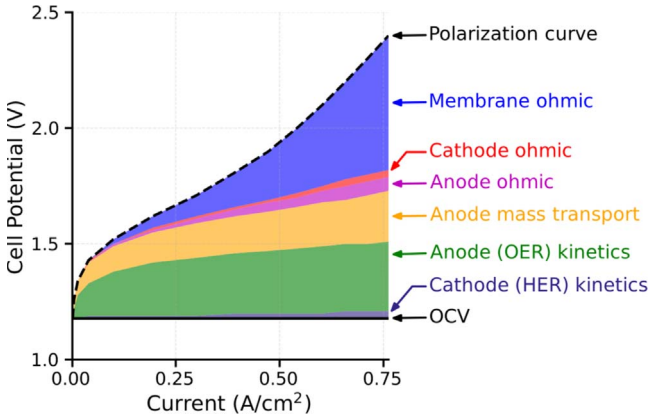

Figure 8. Power-loss analysis voltage breakdown for a vapor electrolyzer, adapted from Ref. 31.

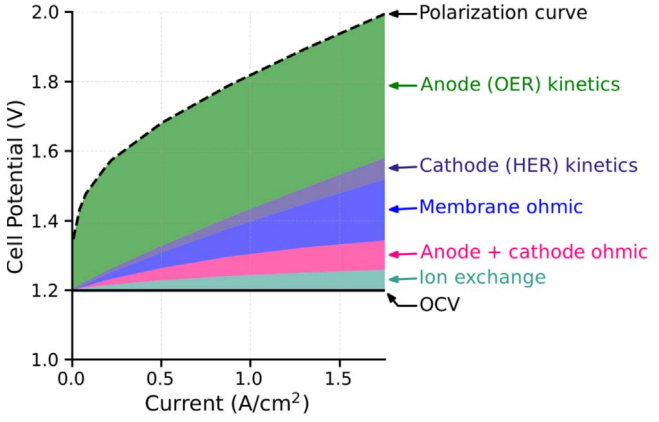

Figure 9. Power-loss analysis voltage breakdown for an AEM electrolyzer. The bottom section indicates the voltage loss corresponding to ion-exchange between the liquid electrolyte and ionomer.

the analysis and it is shown how to adapt the above methodology to account for these additional phenomena.

Proton-exchange-membrane electrolysis.—The key differences between a PEM electrolyzer and a PEM fuel cell are the use of liquid water as a reactant in the PEM electrolyzer and the reversal of the reactions. Accordingly, the hydrogen electrode becomes the cathode and the oxygen electrode becomes the anode, which is reflected in the definitions of the various voltage losses. Therefore, the anode kinetic losses typically become the largest contributor to voltage loss, rather than the cathode kinetic losses. As shown in Fig. 7, the anode kinetics and the ohmic losses within the membrane are the largest losses within the PEME, which coincides with experimental findings. Mass-transport losses are negligible in PEM electrolyzers due to the use of liquid water as the reactant and currently used highly loaded anode catalyst layers (>0.5 mg cm^{-2}).[35]

The power-loss analysis can provide further insight for vapor electrolysis, in which membrane hydration effects become much more important. Fig. 8, adapted from Fornaciari et al.,[31] shows a voltage breakdown of a 2-D model of a vapor electrolyzer indicating mass-transport losses throughout the current-density range. For fuel cells, mass-transport voltage losses typically appear significant only at higher current densities, at which the oxygen concentration in the catalyst layer drops to zero. In Fig. 8, the mass-transport losses appear earlier due to water-vapor transport within the porous, heterogeneous catalyst layers. Understanding the loss as mass transport provides essential information on how to ameliorate it in the catalyst layer, design better electrodes, and provide more reactant to the system.

In both liquid and vapor electrolyzers, voltage breakdowns provide insight on better cell operation. Process conditions such as temperature, humidity, and flow rate can change the breakdowns accordingly as the kinetic, ohmic, and mass transport regimes are dependent on these inputs. Understanding and mitigating these losses could provide better long-term performance by decreasing overpotentials within the cell. As shown in Fig. 8, the vapor electrolyzer has an increased anode mass transport voltage loss relative to the liquid electrolyzer shown in Fig. 8. This voltage loss could be alleviated if better water transport were achieved by using different porous transport layers, more uniform catalyst layers, or more water. This mass transport voltage loss is unique to the vapor electrolysis system and provides an area to improve the technology that may not have been as easily identifiable from the polarization curve alone. Additionally, if new catalysts, thinner membranes tolerant to high differential pressure, or better catalyst layers can be achieved, voltage breakdowns could be used to quantify the improvement.

Anion-exchange membrane electrolysis.—The addition of an electrolyte salt to electrolysis cells has been used to reduce voltage losses, particularly in AEM electrolyzers, in which various salts have been shown to improve performance over that of pure water.[36–38] The additional electrolyte salts are thought to improve ionic conductivity within the catalyst layer and enable the reaction at the catalyst/liquid-electrolyte interface, effectively increasing electrochemically active surface area and reducing kinetic voltage loss. The chemical composition of the electrolyte and its concentration may affect the exchange current density of the electrochemical reactions in the electrolyzer as well.[39]

One of the challenges in modeling AEM electrolyzer performance is the existence of multiple parallel ion-conducting pathways with differing environments that may lead to differing ionic potentials within each pathway. Accurately accounting for the voltage losses due to parallel ion-conduction pathways is critical for understanding and optimizing performance. One source of voltage loss comes from ion exchange between the liquid electrolyte and ionomer. The ion-exchange rate between the ionomer and liquid electrolyte is derived from Donnan equilibrium,[38]

$$R_{exchange} = k_{exchange}\left(c_j^I \exp\left(\frac{z_j F(\phi_I - \phi_L)}{RT}\right) - c_j^L\right), \qquad [25]$$

in which $k_{exchange}$ is an arbitrarily large rate constant, ϕ_I and ϕ_L represent the ionomer and liquid electrolyte potentials, c_j^I and c_j^L represent the concentration of ion j in the ionomer and liquid electrolyte, and z_j represents the charge of ion j. The voltage loss

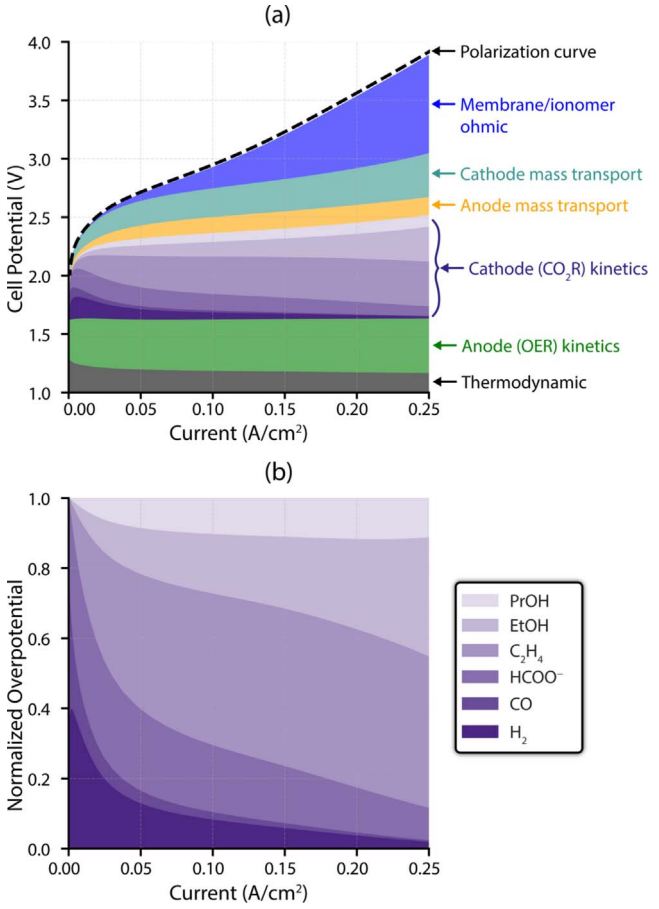

Figure 10. (a) The voltage breakdown of a CO_2 electrolyzer. The unusual membrane ohmic voltage loss increase arises from dryout due to the vapor-fed anode as discussed in detail in Weng et al.[30] (b) The fractional contribution of each electrochemical reaction to the total cathode kinetic overpotential, labeled by product.

corresponding to this ion-exchange process is given by

$$\Delta V_{ion-exchange} = \frac{\int (R_{exchange} z_j F(\phi_I - \phi_L))}{I_{cell}} \quad [26]$$

Figure 9 shows the power-loss analysis voltage breakdown for a 1-D model of an AEM electrolysis cell using 1 M KOH solution as the liquid electrolyte. The grey section indicates the voltage loss induced by ion-exchange power loss. By adding this power loss, the energy conservation is complete, and the voltage losses sum to the total voltage loss. This framework can be extended to other electrolyzers using other electrolytes, such as potassium carbonate.

The power-loss post-processing method breaks down the total voltage loss into different processes in the AEM electrolyzers and provides insight on performance optimization. However, when interpreting the results from this method, one should keep in mind that a larger voltage loss from a single process does not necessarily mean a decrease in performance as all the processes are coupled. For example, the ion-exchange voltage loss increases when the KOH concentration in the liquid electrolyte increases because more current is conducted through the liquid electrolyte, increasing the amount of ion-exchange between the ionomer and the liquid electrolyte. However, the high concentration of KOH in the liquid electrolyte also helps to deliver ions through the catalyst layer, which reduces the catalyst layer ohmic loss. More importantly, the high KOH concentration in the liquid electrolyte facilitates the reaction at the catalyst/liquid-electrolyte interface, which largely reduces the anode kinetic loss. As a result, increasing the KOH concentration benefits the overall electrolyzer performance, even though it increases the ion-exchange voltage loss. Nevertheless, accurately accounting for this ion-exchange loss is essential for understanding the parallel ion-conduction pathways in the AEM electrolyzers.

CO_2-reduction electrolysis.—Understanding the mechanisms of voltage loss in MEA-based systems for electrochemical CO_2 reduction is critical to developing optimized devices that can convert CO_2 to value-added products. The power-loss analysis described above was also applied to a 1-D model of an electrolysis device for the electrochemical reduction of CO_2 using a vapor-fed anode. The model, which is described more fully in the prior work by Weng et al.,[30,40] differs from the fuel-cell and electrolyzer models discussed earlier in that multiple electrochemical reactions are possible and expected at the cathode. When performing CO_2 reduction on a copper catalyst, a wide variety of different hydrocarbon products can be formed, and the reactions to form these products are thus in direct competition in the cathode catalyst layer.[41] In electrochemical CO_2 reduction systems, or any electrochemical system with multiple competing electrochemical reactions, there can be significantly more kinetic and transport parameters than the traditional hydrogen fuel cell or water electrolyzer. Therefore, postprocessing methods are particularly well-suited to these systems because they can deconvolute voltage losses from each electrochemical reaction without recomputing the model for each reaction.

The power-loss method described above can be easily adjusted to separate the kinetic and mass-transport losses associated with each reaction as follows. First, the thermodynamic cell voltage U^0 must be adjusted to reflect the free energy change for the product mixture at the cathode,

$$U^0 = E^0_{anode} - E^0_{cathode} = E^0_{SHE} - \sum_m (FE)_m E^0_m, \quad [27]$$

where E^0_m is the standard reduction potential of reaction m, $(FE)m$ represents the Faradaic efficiency for reaction m, and E^0_{SHE} is the standard reduction potential for the hydrogen reduction reaction, which can also be replaced by a mixture of standard reduction potentials if multiple reactions are expected at the anode.

The deconvolution of the cathodic voltage losses from each electrochemical reaction is shown in Fig. 10, which depicts the voltage breakdown (Fig. 10a) for the 1-D CO_2-electrolyzer model and a further breakdown of the kinetic voltage losses at the cathode into the normalized voltage-loss contributions (Fig. 10b) resulting from the competing CO_2 reduction reactions modeled. Interestingly, when compared to plots of the Faradaic efficiency (defined as the partial current density for a given reaction divided by total current density in the cathode catalyst layer) of the various reactions (Supporting Fig. S1 available online at stacks.iop.org/JES/168/074503/mmedia), the normalized kinetic voltage loss of a given reaction correlates well with its selectivity. In modeling the electrochemical reduction of CO_2 over a copper catalyst, the relative contributions of each reaction to the cathodic kinetic voltage loss are sensitive to the experimental dataset from which the kinetic parameters (exchange current densities and cathodic transfer coefficients) are fit. Thorough models of these systems should use parameters fit across multiple experimental datasets to ensure generalizability of observed trends in the voltage efficiency and selectivity of the individual reactions. The voltage breakdown and selectivity trends shown here use kinetic parameters fit from work by Ebaid et al.,[42] and the trends observed were found to be generalizable over multiple kinetic datasets in the original work by Weng et al.[30]

Additionally, due to the dependence of the thermodynamic cell voltage on the FEs of the individual CO_2-reduction reactions, the

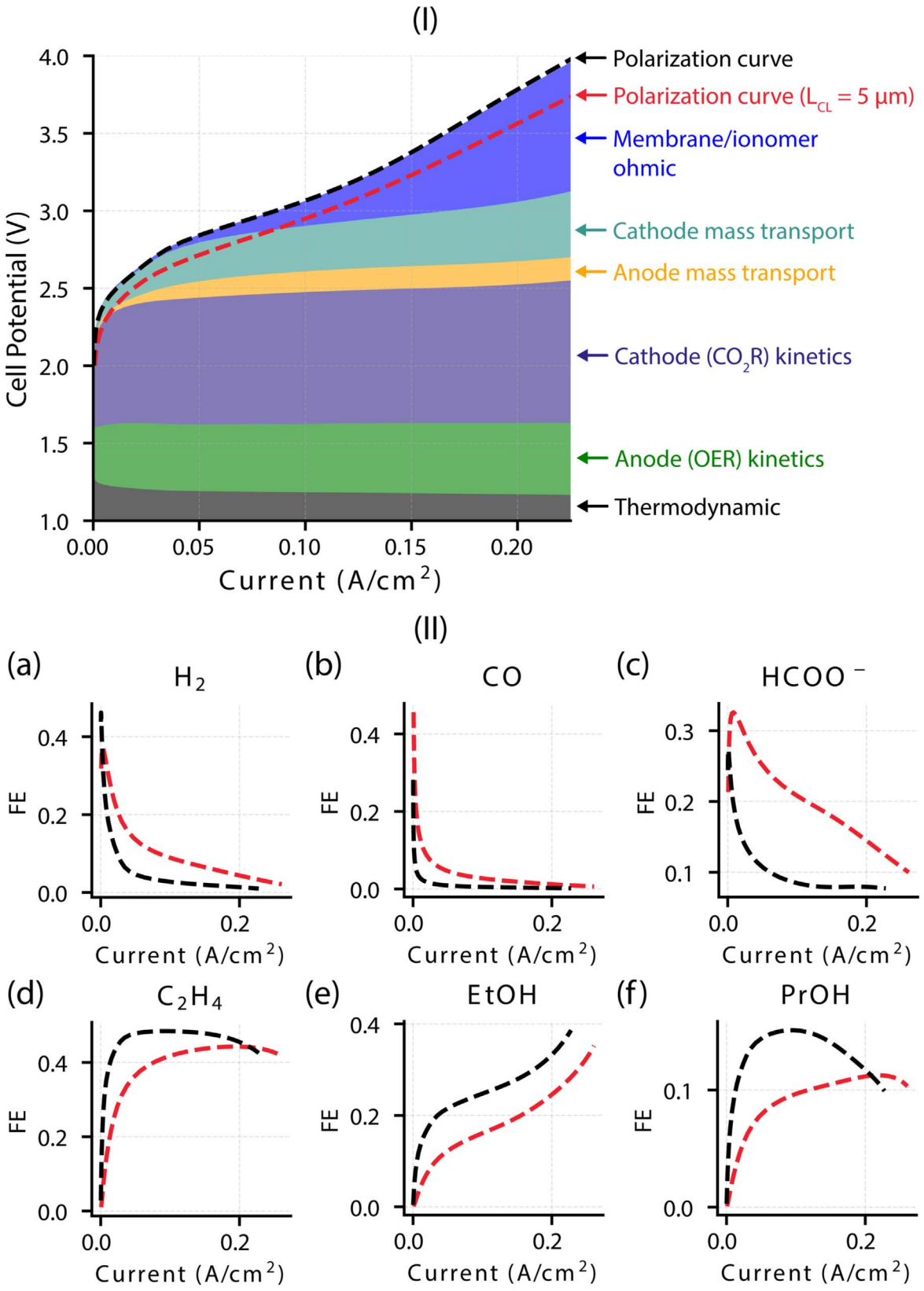

Figure 11. (I) The effect of reducing the cCL thickness from 5 to 0.5 μm on the IV-characteristics of a CO_2 electrolyzer utilizing a copper catalyst. Overall polarization curve from original 5 μm cCL is shown in red dashes. (II)) Faradaic efficiencies to various hydrocarbon products (a)–(f) as a function of applied current for both 5 μm (red dashed lines) and 0.5 μm (black dashed lines) thick cCL.

thermodynamic cell voltage will vary with total current density to reflect changes in the product distribution at the cathode. As the current increases, the FEs for C_{2+} products (that is, products containing two or more carbon atoms) increase. These products typically have more positive standard reduction potentials, and, thus, E^o_{cathode} increases and U^0 decreases.[1] This change of the

thermodynamic cell voltage with applied current is unique to electrochemical systems with multiple competing reactions and can be observed in Fig. 10 as a decrease in the thermodynamic contribution to the voltage breakdown.

Lastly, while voltage-breakdown analysis is typically used to assess the mechanisms of voltage loss in an electrochemical system, when applied to an electrochemical system with multiple competing reactions, this analysis can also be used to explain changes in the FE for certain products that the polarization curve alone cannot assess. For example, as shown in Fig. 11, decreasing the cathode catalyst layer (cCL) thickness from 5 to 0.5 μm results in only a minimal change in the polarization curve (Fig. 11(I)) but significantly improves the selectivity for C_{2+} products (Fig. 11(II)). This improvement in selectivity can be attributed to the increased kinetic overpotential ($\sim$100–150 mV) due to the lower catalyst loading of a thinner cCL[1] and can be observed in the voltage breakdown in Fig. 11(I). The increase in the kinetic overpotential disproportionately improves generation of C_{2+} products because their reactions have larger cathodic transfer coefficients, and thus, their FEs increase at a faster rate with increasing kinetic overpotential in comparison to hydrogen or C_1 products (products with only one carbon atom).[40] Again, the voltage-breakdown analysis provides insights to the selectivity and performance of a CO_2 electrolyzer that would be difficult to intuit when only considering the polarization curve.

Conclusions

Many electrochemical systems can be characterized by polarization curves, which report the overall cell voltage as a function of applied current. Generally, the cell voltage deviates from its ideal thermodynamic value when the applied current is nonzero. Minimizing this voltage deviation maximizes the efficiency of the electrochemical system. These voltage deviations can be understood, and their mechanisms identified, by using mathematical models or guided experiments to generate voltage breakdowns.

In this work, we reviewed several voltage-breakdown methods. Each method has advantages, but no method is unquestionably superior in all situations. Analytical 0-D methods are best suited to rapid analysis or quick fitting of experimental data but cannot provide the in-depth insight or predictiveness of high-fidelity multiphysics simulations. Computational models can be analyzed using a limiting-case approach, in which models are re-computed with new values for the coefficients controlling each type of voltage loss, or they can be analyzed using a post-processing approach, in which an energy balance is used to calculate power losses and thereby calculate voltage losses. Limiting-case methods quantitatively answer design questions, such as "what would be the cell performance if the resistance from mechanism k was eliminated?" and thus have embedded sensitivity analysis. Each limiting-case method has its drawback, however. The cumulative limiting-case method cannot unambiguously determine the voltage breakdown when loss mechanisms are coupled, because the order of removing the loss mechanisms affects the result. On the other hand, the standalone limiting-case method ignores coupling, and therefore cannot quantify the cumulative effect of each mechanism on the cell voltage and hence is more single phenomenon rather than system of phenomena. The power-loss method rapidly analyzes simulations and unambiguously quantifies voltage loss, provided the voltage-loss mechanisms can be clearly defined mathematically. From the perspective of cell engineering, however, the instantaneous value of the voltage loss is less important than understanding what would happen if a material property or cell process was altered. Thus, the power-loss method is descriptive or diagnostic in nature, whereas the limiting-case methods are predictive. With these different approaches, the analysis, albeit complicated, can provide different insights on diagnostics or design criteria. Given the ambiguity of voltage-loss breakdowns in literature, we hope that this work can serve as a common guide and reference for experimentalists and theorists regardless of which method they choose. To illustrate the diagnostic power and flexibility of the post-processing approach, we calculated voltage breakdowns for a variety of electrochemical systems. These breakdowns enrich the discussion of the polarization curves and allow for more intuitive understanding of the limitations of a given electrochemical system.

Acknowledgments

This work was accomplished as part of the Million Mile Fuel Cell Truck (M^2FCT) Consortium and the H2NEW Consortium funded by the Hydrogen and Fuel Cell Technologies Office, of the U.S. Department of Energy, under contract number DE-AC02-05CH11231. We thank Dr Lien-Chun Weng and Anamika Chowdhury for helpful discussions. We also acknowledge interactions with Annex 37 of the Advanced Fuel Cells Technology Collaboration Programme part of the Technology Platform of the IEA. This work was prepared as an account of work sponsored by an agency of the United States Government. The views and opinions of the authors expressed herein do not necessarily state or reflect those of the United States Government or any agency thereof. Neither the United States Government nor any agency thereof, nor any of their employees, makes any warranty, expressed or implied, or assumes any legal liability or responsibility for the accuracy, completeness, or usefulness of any information, apparatus, product, or process disclosed, or represents that its use would not infringe privately owned rights.

ORCID

Michael R. Gerhardt https://orcid.org/0000-0002-1272-3607
Lalit M. Pant https://orcid.org/0000-0002-0432-3902
Justin C. Bui https://orcid.org/0000-0003-4525-957X
Julie C. Fornaciari https://orcid.org/0000-0002-0473-2298
Jiangjin Liu https://orcid.org/0000-0002-1408-4335
Adam Z. Weber https://orcid.org/0000-0002-7749-1624

References

1. L. M. Pant, Z. Yang, M. L. Perry, and A. Z. Weber, *J. Electrochem. Soc.*, **165**, F3007 (2018).
2. J. Newman and K. E. Thomas-Alyea, *Electrochemical Systems* (John Wiley & Sons, Inc., Hoboken, NJ) (2004).
3. D. M. Bernardi and M. W. Verbrugge, *J. Electrochem. Soc.*, **139**, 2477 (1992).
4. C. Marr and X. Li, *ARI-An International Journal for Physical and Engineering Sciences*, **50**, 190 (1997).
5. J. J. Baschuk and X. Li, *J. Power Sources*, **86**, 181 (2000).
6. A. A. Kulikovsky, *J. Electrochem. Soc.*, **161**, F263 (2014).
7. A. A. Kulikovsky, *J. Electrochem. Soc.*, **161**, E3171 (2014).
8. A. Kulikovsky, *Energies*, **7**, 351 (2014).
9. D. Yu and S. Yuvarajan, *J. Power Sources*, **142**, 238 (2005).
10. M. Baghlaha, J. Stumper, and M. Eikerling, *ECS Trans.*, **28**, 159 (2010).
11. R. P. Iczkowski and M. B. Cutlip, *J. Electrochem. Soc.*, **127**, 1433 (1980).
12. M. Secanell, A. Putz, S. Shukla, P. Wardlaw, M. Bhaiya, L. M. Pant, and M. Sabharwal, "Mathematical Modelling and Experimental Analysis of Thin, Low-Loading Fuel Cell Electrodes." *ECS Transactions*, **69**, 157 (2015).
13. A. Kosakian, L. Padilla Urbina, A. Heaman, and M. Secanell, "Understanding single-phase water-management signatures in fuel-cell impedance spectra: A numerical study." *Electrochimica Acta*, **350**, 136204 (2020).
14. H. A. Gasteiger, J. E. Panels, and S. G. Yan, *J. Power Sources*, **127**, 162 (2004).
15. T. J. Omasta et al., *Energy Environ. Sci.*, **11**, 551 (2018).
16. H. A. Gasteiger, W. Gu, R. Makharia, M. F. Mathias, and B. Sompalli, *Handbook of Fuel Cells* (John Wiley & Sons, Ltd., Chichester, United Kingdom) (2010).
17. S. Flick, S. R. Dhanushkodi, and W. Merida, *J. Power Sources*, **280**, 97 (2015).
18. D. L. Wood III and R. L. Borup, *J. Electrochem. Soc.*, **157**, B1251 (2010).
19. M. V. Williams, H. R. Kunz, and J. M. Fenton, *J. Electrochem. Soc.*, **152**, A635 (2005).
20. S. Haji, *Renewable Energy*, **36**, 451 (2011).
21. A. Z. Weber and J. Newman, *Chem. Rev.*, **104**, 4679 (2004).
22. C. E. Chamberlin, P. A. Lehman, R. M. Reid, and T. G. Herron, *Proceedings of the 10th World Hydrogen Energy Conference*, Cocoa Beach, FL, ed. D. Block and T. N. Veziroglu, **3**, 1659 (1994).
23. J. Kim, S.-M. Lee, S. Srinivasan, and C. Chamberlin, *J. Electrochem. Soc.*, **142**, 2670 (1995).
24. J. H. Lee, T. R. Lalk, and A. J. Appleby, *J. Power Sources*, **70**, 258 (1998).
25. U. Beuscher, *J. Electrochem. Soc.*, **153**, A1788 (2006).
26. A. Weber, R. Darling, J. Meyers, and J. Newman, *Handbook of Fuel Cells* (John Wiley & Sons, Ltd., Chichester, UK) (2010).

27. J. Newman, *Electrochim. Acta*, **24**, 223 (1979).
28. L. M. Pant, M. R. Gerhardt, N. Macauley, R. Mukundan, R. L. Borup, and A. Z. Weber, *Electrochim. Acta*, **326** (2019).
29. A. Kusoglu and A. Z. Weber, *Chem. Rev.*, **117**, 987 (2017).
30. L.-C. Weng, A. T. Bell, and A. Z. Weber, *Energy Environ. Sci.*, **13**, 3592 (2020).
31. J. C. Fornaciari, M. R. Gerhardt, J. Zhou, Y. N. Regmi, N. Danilovic, A. T. Bell, and A. Z. Weber, *J. Electrochem. Soc.*, **167** (2020).
32. M. R. Gerhardt, L. M. Pant, and A. Z. Weber, *J. Electrochem. Soc.*, **166**, F3180 (2019).
33. A. Z. Weber and J. Newman, *J. Electrochem. Soc.*, **151**, A311 (2004).
34. M. Moore, P. Wardlaw, P. Dobson, J. J. Boisvert, A. Putz, R. J. Spiteri, and M. Secanell, *J. Electrochem. Soc.*, **161**, E3125 (2014).
35. Z. Taie, X. Peng, D. Kulkarni, I. V. Zenyuk, A. Z. Weber, C. Hagen, and N. Danilovic, *ACS Appl. Mater. Interfaces*, **12**, 52701 (2020).
36. C. C. Pavel, F. Cecconi, C. Emiliani, S. Santiccioli, A. Scaffidi, S. Catanorchi, and M. Comotti, *Angewandte Chemie - International Edition*, **53**, 1378 (2014).
37. H. Ito, N. Kawaguchi, S. Someya, T. Munakata, N. Miyazaki, M. Ishida, and A. Nakano, *Int. J. Hydrogen Energy*, **43**, 17030 (2018).
38. L. N. Stanislaw, M. R. Gerhardt, and A. Z. Weber, *ECS Trans.*, **92**, 767 (2019).
39. D. Li et al., *Nat. Energy*, **5**, 378 (2020).
40. L. C. Weng, A. T. Bell, and A. Z. Weber, *Phys. Chem. Chem. Phys.*, **20**, 16973 (2018).
41. S. Nitopi et al., *Chem. Rev.*, **119**, 7610 (2019).
42. M. Ebaid, K. Jiang, Z. Zhang, W. S. Drisdell, A. T. Bell, and J. K. Cooper, *Chem. Mater.*, **32**, 3304 (2020).